Superhard materials with low elastic moduli: Three-dimensional covalent bonding as the origin of superhardness in B_{6}O

R. F. Zhang, Z. J. Lin, Y. S. Zhao, and S. Veprek

Phys. Rev. B **83**, 092101 — Published 4 March 2011

DOI: 10.1103/PhysRevB.83.092101

Superhard materials with low elastic moduli: Origin of the superhardness in B_6O

R. F. Zhang,[1] Z. J. Lin,[2]* Y. S. Zhao,[2,3] and S. Veprek[1]*

[1]Department of Chemistry, Technical University Munich, Lichtenbergstr. 4, D-85747 Munich, Germany

[2]LANSCE–Lujan Neutron Scattering Center, Los Alamos National Laboratory, Los Alamos, New Mexico 87545, USA

[3]High Pressure Science and Engineering Center, University of Nevada Las Vegas, Nevada 89154, USA

Abstract

Using first-principles calculations, we show that, in spite of its relatively low shear modulus, boron suboxide (B_6O) is superhard because its high shear strength of ≥38 GPa originates from three-dimensional covalently bonded network of B12 icosahedral units connected by boron and oxygen atoms. We further demonstrate that the high shear resistance of B_6O is related to strong B-B covalent bonds which connect the B12 units. These results challenge the concept of design intrinsically superhard materials based on high elastic moduli only.

*E-mail: zlin@lanl.gov *stan.veprek@lrz.tum.de

Indentation hardness H is the average pressure beneath the indenter under the conditions of fully developed plasticity [1]. The irreversible plastic deformation in intrinsically superhard crystalline materials occurs by multiplication and movement of dislocations, both of which are related to shear modulus, G. However, the correlation of hardness with G displays large scatter [2]. Intrinsically superhard materials, such as diamond and c-BN, attain their hardness from strong covalent bonds and isotropic structure, whereas extrinsically superhard materials, such as nc-TiN/a-Si_3N_4 nanocomposites (Hardness, $H \geq 50$ GPa) consisting of 3-4 nm size TiN nanocrystals "glued" together by about one monolayer thick Si_3N_4-like interfacial layer, gain their high hardness from their nanostructure which hinders dislocation activity, and from the strong Si_3N_4 interfacial layer that hinders the grain boundary shear [3-5]. However, the elastic moduli of these materials are relatively low (bulk modulus B=295 GPa, G=190 GPa [6]) as compared with those of c-BN, diamond, and *5d* diborides. In this paper we show why boron suboxide is intrinsically superhard although its elastic moduli are relatively small.

Based on their high elastic moduli, materials, such as C_3N_4 [7], OsB_2 [8,9], ReB_2 [10,11] and others were predicted to be superhard. However, these predictions were not validated by experiments [12,13]. For example, Liu and Cohen [7] predicted that the hardness of C_3N_4 should be close to that of diamond because its calculated bulk modulus was similar. However the experimentally measured hardness of stoichiometric C_3N_4 thin films was below 30 GPa [12]. Recent first-principles calculations showed that its shear strength is limited by electronic instability upon a shear of about ≥ 0.24,

when the non-binding electron pairs on nitrogen interact with carbon orbitals resulting in the formation of double bonds and transformation to graphite-like, soft structure [14]. Much interest has been recently devoted to diborides of *5d* transition metals because of their high elastic moduli (e.g. [11]). Also in these cases, the experimental results do not confirm the prediction: in spite of its very high isotropic elastic moduli (B≈365-395 [8], G≈216 [9]), OsB_2 has hardness of only about 20 GPa because of easy sliding between Os-Os (001) layers having very low shear strength of only 9.1 GPa (7.2 GPa for pure iron) [10]. ReB_2 has load invariant hardness of less than 30 GPa [11,13] because, upon finite shear, it undergoes a series of electronic instabilities and transformation to metastable phases with lower shear resistance than that of the equilibrium structure [15].

These few examples illustrate that achieving intrinsic superhardness requires electronic and structural stability upon large shear strain [15,16]. Instabilities due to interaction of non-binding electron pairs with unfilled orbitals of other atoms in the crystal as found for C_3N_4 [14], or due to soft metal-metal bonds as in OsB_2 [10], or due to crystal field splitting as found in ReB_2 [15] are likely to be fairly general features which are limiting the strength and hardness of many ultra-incompressible materials. In this paper, we show that although the elastic moduli of B_6O are lower than those of C_3N_4 and of all 5*d* diborides, it is intrinsically much harder because of a strong, fairly isotropic three-dimensional covalent boron network which withstands large shear strain.

Badzian reported the preparation of a range of boron suboxides with different

stoichiometries and hardness varying between 32 and 60 GPa (38.2 GPa for B_6O) [17]. In spite of large scatter of the hardness data of boron suboxides due to a poor control of the stoichiometry and compaction, the hardness of B_6O polycrystalline compacts exceeds 40 GPa ([18] p. XL, LXV, 9 and 526) and reaches 45 GPa for single crystals [19], which is close to that of c-BN (about 48 GPa [3]). Furthermore, hot pressed boron suboxide displays lower bulk (B=230 GPa) and shear (G=206 GPa) moduli [20] (bulk modulus of B_6O single crystal is 270 GPa [21]) than those of OsB_2 (B≈365-395 GPa, G≈216 GPa) [8,9], ReB_2 (B=348 GPa, G=274 GPa) [22] and c-BN (B=376 GPa, G=390 GPa) [22]. Properties of B_6O close to equilibrium (i.e. valence charge density and elastic moduli) have been widely used to explain its superhardness (see e.g. [18] [23] and references therein). However, the above mentioned examples show that high values of elastic moduli and valence charge density in equilibrium do not guarantee high hardness, which is measured under conditions of fully developed plasticity. Instead, it is much more demanding to study the electronic structure and deformation mechanism in shear far from equilibrium.

Our first-principles calculations were performed using the VASP code [24] with the generalized-gradient approximation proposed by Perdew and Wang for exchange-correlation functional. The integration in the Brillouin zone was employed using the Monkhorst-Pack scheme (5×5×3), energy cutoff of 600 eV, and tetrahedron method with Blöchl corrections for the energy calculation and Gaussian smearing for the stress calculations, respectively. The conjugate gradient method was used for the relaxation of structural parameters. Details of our stress-strain calculations can be

found in Refs. [22,25].

The calculations were performed with 42-atom B_6O unit cell in hexagonal representation. Four Miller-Bravais indices were used with $x<10\bar{1}0>$, $y<\bar{1}2\bar{1}0>$ and $z<0001>$ directions for tension, and on $(10\bar{1}0)<\bar{1}2\bar{1}0>$, $(0001)<\bar{1}2\bar{1}0>$, and $(0001)<10\bar{1}0>$ slip systems for shear. The calculated lattice constants in hexagonal representation of a=0.5391 nm, c=1.2312 nm and bulk modulus of B=230 GPa for B_6O are in agreement with the previous calculated and experimental (in parentheses) data: a=0.5331 nm [21] (0.5397 nm [26]), c=1.2124 nm [21] (1.2317 nm [26]), and B=222 GPa [27] (230 GPa [20]). The bulk modulus of B_6O is much lower than that of c-BN (377 GPa) [25], OsB_2 (365-395 GPa) [8] and h-ReB_2 (348 GPa) [22], indicating a higher compressibility of the former. The Voigt shear modulus G_v of B_6O derived from the calculated anisotropic elastic constants is also much lower than those of h-ReB_2 and c-BN (see Table I [21,22,25-28]), indicating a lower stiffness of B_6O.

In order to assess the bonding strength of a crystal, one has to explore electronic and structural stabilities at large strains which yield the ideal strengths, because electronic instabilities at large strain can result in structural transformations to phases with a lower shear resistance than that of the equilibrium phase described by its elastic modulus [14,15,29]. Figure 1 shows (a) the calculated stress-strain curves and (b) the structure and crystallographic orientation of B_6O. The calculated anisotropic ideal strengths are also summarized in Table I and compared with those for h-ReB_2, c-BN, and Diamond [16,22,25,28,30]. The anisotropy ratio for B_6O of $\sigma_{<\bar{1}2\bar{1}0>}=68.9$ GPa: $\sigma_{<0001>}=61.9$ GPa: $\sigma_{<10\bar{1}0>}=53.3$ GPa comes up as 1.29 : 1.16 : 1, which is

lower than the corresponding values of both c-BN of $\sigma_{<1\bar{1}0>} = 84.1$ GPa : $\sigma_{<\bar{1}\bar{1}2>} = 60.3$ GPa : $\sigma_{<111>} = 55.3$ GPa with a ratio of 1.53 : 1.09 : 1, and of h-ReB_2 of $\sigma_{<0001>} = 93.2$ GPa : $\sigma_{<10\bar{1}0>} = 63.8$ GPa : $\sigma_{<\bar{1}2\bar{1}0>} = 58.5$ GPa with a ratio of 1.59 : 1.09 : 1. This fairly isotropic bond strength of the B_6O is seen in Fig. 1(b) as three-dimensional cage-like B-network of icosahedral B_{12} units connected by oxygen atoms. The calculated ideal shear strength of the B_6O of τ_{xz}=38 GPa to τ_{yz}=42 GPa along the *xz* and *yz* shear is lower than that of the c-BN of 58 to 65 GPa in the (111) slip plane, but higher than that of h-ReB_2 of 34 GPa in (0001) slip plane (see Table I). The resolved zero-pressure anisotropic shear modulus of B_6O along the weakest slip system of about 173 GPa is much lower than that of h-ReB_2 (257 GPa) [22]. Thus, in spite of its significantly higher shear modulus, h-ReB_2 has lower shear strength than B_6O, because upon a finite shear strain it undergoes electronic instabilities and structural transformation to metastable phases with a lower shear resistance [15].

To obtain deeper understanding of the origin of the mechanical properties of B_6O, we calculated the electronic density of states (DOS) and valence charge density difference (VCDD) defined as the difference between the calculated total valence charge density of the crystal minus the charge densities of neutral atoms. It is seen from Fig 2 (a) that the total DOS of B_6O displays three regions: the valence band is dominated by B 2*s* states at low energies, by O 2*p* states in the middle range and B 2*p*-like states at the higher energies. The calculated band gap of about 2.4 eV is in agreement with that reported in Ref. [31] (2.4 eV). Fig. 2 (b) shows the VCDD in the $(11\bar{2}0)$ plane of B_6O. Positive value (white color and solid contours) means an increase while negative value

(blue color and dotted contours) indicates a decrease of the negative charge as compared to neutral atoms. The strong directional bonds between B-O pairs can be seen as a significant charge transfer from B to O [white color regions at the O atoms in Fig. 2(b)]. The strong covalent B-B bonds in cage-like boron network are seen as charge accumulation [see also the isosurfaces of VCDD shown in Fig. 1(b)].

To further quantify the charge transfer of B_6O, we analyzed the charge density by the method of Bader [32] using the code developed by Henkelman et al. [33]. The results yield an average charge of $B^{1.53}O^{-1.53}$, i.e. a relatively strong polarity of the B-O bonds. The relatively high VCCD between B-O bonds and nearly isotropic, three-dimensional covalent B-B-cages explain the origin of its higher shear resistance.

Figure 3 shows the structure of B_6O before and after lattice instability under the weakest $(0001)<10\bar{1}0>$ shear deformation [cf. Fig. 1(a)]. It can be seen that the covalent B1-B2 and B3-B4 bonds, which connect the B12 units, become unstable at the peak shear stress of 38 GPa and strain of 0.35. During the shear, the B1-B2 bonds "flip over" from left to right, while the B3-B4 bond length increases from 0.17 nm at equilibrium, to 0.23 nm at peak stress, and to 0.35 nm at strain of 0.5558. However, the three-dimensional B_{12} units remain intact after the peak stress, and neither lattice collapse nor phase transformation occur even at a highest shear strain. Obviously, the B-B bonds connecting the B12 units determine the mechanical properties of B_6O upon shear. In ReB_2 however, the two-dimensional, buckled sixfold boron rings are intercalated by Re layers that have partial metallic bonding, which allows an easier shear and phase transformations, as reported in Refs. [15,16]. This relatively easy

sliding of the two-dimensional boron layers between the Re-layers limits the achievable strength and hardness of ReB_2.

In summary, we studied the intrinsic mechanical and electronic properties of B_6O and compared them with those of superhard c-BN and hard OsB_2 and ReB_2. Our results show that, in spite of its lower elastic moduli, B_6O possesses higher shear strength as compared to OsB_2 and ReB_2 because of its three-dimensional, almost isotropic, covalently bonded boron cage-like structure. Therefore, although more compressible (lower B) and less rigid (lower G), B_6O is intrinsically much harder than OsB_2 and ReB_2. Also the recently reported superhard (H=58 GPa) but compressible (B_v≈227 GPa) high-pressure phase of boron [34], and well known boron carbide (H≥40 GPa [18] Table I, p. 968, B_v=224 GPa [23,27] [recently, Z. J. Lin calculated the elastic moduli of these materials and obtained similar values; unpublished]) consisting of a three-dimensional network of B_{12} icosahedra connected by B_2 bridges support our conclusion: not high elastic moduli at infinitesimal strain, but strong covalently bonded three-dimensional, isotropic network, as shown here for B_6O, may assure high intrinsic hardness of a material. Alternatively, nanosized materials with crystallite size of 10-30 nm that are strengthened by absence of dislocation activity can achieve hardness enhancement by a factor of ≤2 as compared to the intrinsic hardness of coarse-grained ones (see e.g. Refs. [3,35,29]). An appropriately designed nanostructural materials with strengthened interface that avoids the grain boundary shear can assure such materials to be extrinsically ultrahard, reaching hardness of 50 to >100 GPa [4,5,16,29] and finding many industrial applications [29].

Acknowledgment

We would like to thank Prof. A. S. Argon and Dr. Maritza Veprek-Heijman for helpful comments to the manuscript and Prof. G. Kresse for valuable advice for the application of VASP. Work at Los Alamos is supported by Los Alamos National Security LLC under DOE contact DEAC52-06NA25396.

Reference

[1] G. Tabor, *The Hardness of Metals* (Clarendon Press, Oxford 1951)

[2] D.M. Teter, MRS Bull. **23**, 22 (1998).

[3] S. Veprek, J. Vac. Sci. Technol. A **17**, 2401 (1999).

[4] S. Veprek, M.G.J. Veprek-Heijman, P. Karvankova, and J. Prochazka, Thin Solid Films **476**, 1 (2005).

[5] R.F. Zhang, A.S. Argon, and S. Veprek, Phys. Rev. Lett. **102**, 015503 (2009); Phys. Rev. B **80**, 233401 (2009); B **81**, 254418 (2010).

[6] S. Veprek, S.G. Prilliman, and S.M. Clark, J. Phys. Chem. Solids **71**, 1175 (2010).

[7] A.Y. Liu and M.L. Cohen, Science **245**, 841 (1989).

[8] R.W. Cumberland, M.B. Weinberger, J.J. Gilman, S.M. Clark, S.H. Tolbert and R.B. Kaner, J. Am. Chem. Soc. **127**, 7264 (2005).

[9] X.-Q. Chen, C.L. Fu, M. Krcmar and G.S. Painter, Phys. Rev. Lett. **100**, 196403 (2008).

[10] J. Yang, H. Sun, and C.F. Chen, J. Am. Chem. Soc. **130**, 7200 (2008).

[11] H.Y. Chung, M.B. Weinberger, J.B. Levine, A. Kavner, J.M. Yang, S.H. Tolbert, and R.B. Kaner, Science **316,** 436 (2007).

[12] S. Veprek, J. Weidemann, and F. Glatz, J. Vac. Sci. Technol. A **13**, 2914 (1995).

[13] N. Dubrovinskaia, L. Dubrovinsky, and V.L. Solozhenko, Science **318**, 1550 (2007).

[14] Y. Zhang, H. Sun, and C. Chen, Phys. Rev. B **73**, 064109 (2006).

[15] R.F. Zhang, D. Legut, R. Niewa, A.S. Argon, and S. Veprek, Phys. Rev. B **82**,

104104 (2010).

[16] S. Veprek, A.S. Argon, and R.F. Zhang, Philos. Mag. **90**, 4101 (2010).

[17] A.R. Badzian, Appl. Phys. Lett. **53**, 2495 (1988).

[18] R. Riedel, editor, *Handbook of Ceramic Hard Materials* (Wiley, Weinheim, 2000).

[19] D.W. He, Y.S. Zhao, L. Daemen, J. Qian, T.D. Shen, and T.W. Zerda, Appl. Phys. Lett. **81**, 643 (2002).

[20] D.R. Petrak, R. Ruh, and G.R. Atkins, Am. Ceram. Soc. Bull. **83**, 569 (1974).

[21] D.W. He, S.R. Shieh, and T.S. Duffy, Phys. Rev. B **70**, 184121 (2004).

[22] R.F. Zhang, S. Veprek, and A.S. Argon, Appl. Phys. Lett. **91**, 201914 (2007).

[23] X.J. Guo, J.L. He, Z.Y. Liu, Y.J. Tian, J. Sun and H.T. Wang, Phys. Rev. B **73**, 104115 (2006).

[24] G. Kresse and J. Furthmüller, Comput. Mater. Sci. **6,** 15 (1996).

[25] R.F. Zhang, S. Veprek, and A.S. Argon, Phys. Rev. B **77**, 172103 (2008).

[26] Y.P. Lu and D.W. He, J. Appl. Phys. **105**, 083540 (2009).

[27] S. Lee, D.M. Bylander, and L. Kleinman, Phys. Rev. B **45**, 3245 (1992).

[28] C. Jiang, Z.J. Lin, J.Z. Zhang, and Y.S. Zhao, Appl. Phys. Lett. **94**, 191906 (2009).

[29] S. Veprek, invited review, J. Nanosci. Nanotechnol. **11**, 14 (2011).

[30] H.J. McSkimin and P. Andreatch, Jr., J. Appl. Phys. **43**, 2944 (1972).

[31] D. Li and W.Y. Ching, Phys. Rev. B **54**, 1451 (1992).

[32] R.F.W. Bader, *Atoms in Molecules-A Quantum Theory* ,Oxford University Press, Oxford, 1990.

[33] G. Henkelman, A. Arnaldsson, and H. Jónsson, Comput. Mater. Sci. **36**, 354 (2006).

[34] E.Yu. Zarechnaya, L. Dubrovinsky, N. Dubrovinskaia, et al., Phys. Rev. Lett. **102**, 185501 (2009).

[35] N. Dubrovinskaia, V.L. Solozhenko, M. Miyaima et al., Appl. Phys. Lett. **90**, 101912 (2007).

TABLE I. Summary of Single crystal elastic constants c_{ij}, Voigt bulk modulus B_v, Voigt shear modulus G_v and ideal strengths (minimum shear modulus G_{min}, tensile strength $\boldsymbol{\sigma}_{min}$, and shear strength $\boldsymbol{\tau}_{min}$) for B_6O calculated from first-principles and compared with those of $B_{13}C_2$, h-ReB_2 [22], γ-B_{28} [28], c-BN [25], and diamond [16,30] (all in GPa).

Material	c_{11}	c_{33}	c_{12}	c_{13}	c_{44}	B_v	G_v	G_{min}	$\boldsymbol{\sigma}_{min}$	$\boldsymbol{\tau}_{min}$
B_6O	603	459	109	50	179	231	218	173	$\sigma_{<10\bar{1}0>}=53.3$	$\tau_{(0001)<10\bar{1}0>}=38.0$
$B_{13}C_2$	517	453	118	73	114	224	167	115	$\sigma_{<10\bar{1}0>}=62.4$	$\tau_{(0001)<10\bar{1}0>}=39.4$
h-ReB_2	631	1015	158	134	257	348	274	257	$\sigma_{<\bar{1}2\bar{1}0>}=58.5$	$\tau_{(0001)<10\bar{1}0>}=34.4$
γ-B_{28}	609	456	84	42	241	224	236		$\sigma_{<010>}=51.0$	
c-BN	786		172		445	376	390	324	$\sigma_{<111>}=55.3$	$\tau_{(111)<11\bar{2}>}=58.3$
Diamond	1079		124		578	442	528	471	$\sigma_{<111>}=82.3$	$\tau_{(111)<11\bar{2}>}=86.8$

Figure Captions:

FIG. 1. (Color online) (a) Stress-strain relationships and (b) crystallographic orientation and structure of B_6O calculated by *ab initio* density functional theory. The isosurfaces correspond to valence charge density difference of 0.015 electrons/Bohr^3, the larger green and smaller red spheres represent boron and oxygen atoms, respectively.

FIG. 2. (Color online) (a) Total and partial electronic density of state and (b) The valence charge density difference on the $(11\bar{2}0)$ plane for B_6O. The dashed line indicates the Fermi level. The valence charge density difference scale runs from -0.024 (blue, dark in black and white) to 0.103 electrons/Bohr^3 (white).

FIG. 3. (Color online) Structure of B_6O at shear strain of (a) γ=0.3278 and (b) γ=0.5558 in the $(0001)<10\bar{1}0>$ slip system. The large and small spheres represent B and O atoms, respectively. The blue arrowheads indicate the instability of B3-B4 bonds upon shear.

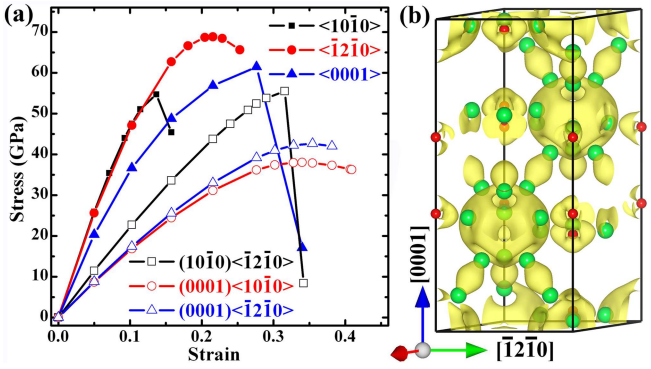

Figure 1 LW12271 18JAN2011

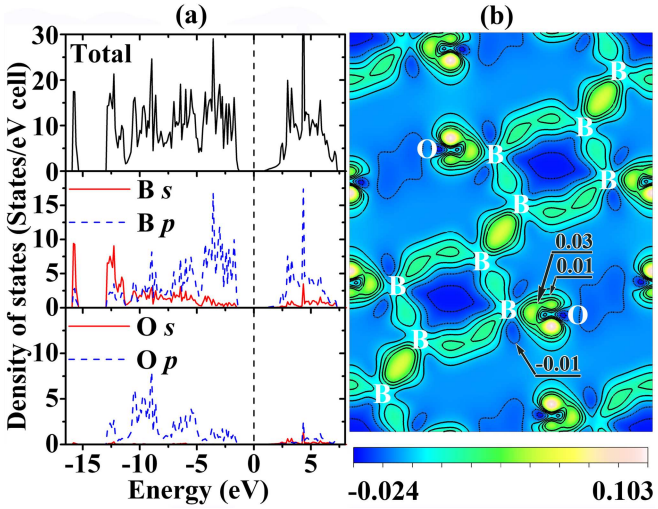

Figure 2 LW12271 18JAN2011

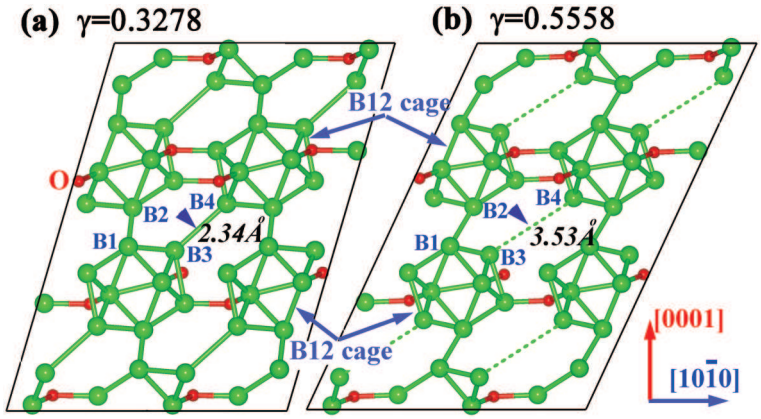

Figure 3 LW12271 18JAN2011